Chaotic properties of planar elongational flow and planar shear flow: Lyapunov exponents, conjugate-pairing rule, and phase space contraction

Federico Frascoli,[1] Debra J. Searles,[2,*] and B. D. Todd[1,†]

[1]*Centre for Molecular Simulation, Swinburne University of Technology, P.O. Box 218, Hawthorn, Victoria 3122, Australia*

[2]*School of Science, Griffith University, Brisbane, Queensland 4111, Australia*

The simulation of planar elongational flow in a nonequilibrium steady state for arbitrarily long times has recently been made possible, combining the SLLOD algorithm with periodic boundary conditions for the simulation box. We address the fundamental questions regarding the chaotic behavior of this type of flow, comparing its chaotic properties with those of the well-established SLLOD algorithm for planar shear flow. The spectra of Lyapunov exponents are analyzed for a number of state points where the energy dissipation is the same for both flows, simulating a nonequilibrium steady state for isoenergetic and isokinetic constrained dynamics. We test the conjugate-pairing rule and confirm its validity for planar elongation flow, as is expected from the Hamiltonian nature of the adiabatic equations of motion. Remarks about the chaoticity of the convective part of the flows, the link between Lyapunov exponents and viscosity, and phase space contraction for both flows complete the study.

I. INTRODUCTION

For the last 15 years, there has been a continuous interest in the chaotic behavior of many-body systems in the framework of nonequilibrium molecular dynamics (NEMD) [1–6]. In this sense, one of the most widely accepted requirements for a system to be chaotic is that it has at least one positive Lyapunov exponent. Lyapunov exponents measure the mean exponential rate of expansion and contraction of initially nearby phase space trajectories. Not only do they provide information about the geometry of the phase space, but they can also be used to extract the values of some key dynamical quantities of the system, such as viscosity and entropy production rate.

In this study, we present the Lyapunov spectra for nonequilibrium steady state systems of simple atoms interacting via a pairwise additive Weeks-Chandler-Anderson (WCA) potential [7] and subjected to either planar shear flow (PSF) or planar elongational flow (PEF). In the former case, we simulate a planar Couette flow regime via the well-established non-Hamiltonian SLLOD algorithm and Lees-Edwards periodic boundary conditions (PBCS) [8]. In the latter, we employ the Hamiltonian SLLOD algorithm for PEF with "deforming-brick" PBCS [9–11] and use an Arnold cat map scheme [12,13] to impose the periodicity relations on the unit lattice. The cat map was recently shown [12] to be related to the Kraynik-Reinelt conditions [14] for the compatibility and reproducibility of the simulation box.

Since heat must be periodically removed from the system for it to reach a steady state, we use Gauss' principle of least constraint [8] to keep either the kinetic temperature or the total energy of the system constant, via a thermostat or an ergostat. To our knowledge these are the first results for the Lyapunov spectrum for a system in a steady state subjected to an elongational flow.

A very interesting property of a dynamical system is the so-called conjugate-pairing rule (CPR), which reflects the symmetry of its Lyapunov spectrum. If we order the exponents according to their value and form pairs coupling the highest with the lowest, the second highest with the second lowest, and so on, the CPR is satisfied when each sum of pairs has the same value. As repeatedly stressed in the literature, the satisfaction of this property is not only important *per se*, but it leads to a dramatic reduction in the amount of calculation required to compute the dynamical properties of the system related to the sum of the exponents.

It is still under debate [15–17] if the SLLOD algorithm for PSF effectively satisfies the CPR, as any formal proof for the existence of sufficient conditions for the CPR to hold is lacking. In this sense, we shall see that our results suggest PEF obeys CPR in the thermodynamic limit whereas CPR is violated in PSF. This is understandable from the fact that the structure of the adiabatic (i.e., without the thermostat or ergostat term) equations of motion is not symplectic for the latter (see Ref. [6] for a discussion on the effect of adding a thermostatting or ergostatting term to the equations of motion).

The paper is organized as follows. In Sec. II we revise the features of PSF and PEF and their algorithms, along with some of the dynamical properties of the systems under consideration. In Sec. III we describe the procedure for the computation of Lyapunov exponents, illustrate the connections between the exponents and nonequilibrium viscosity, and give indications about the exponents associated with the conserved properties of the systems under study. In Sec. IV we present and discuss our results for isokinetic (IK) and isoenergetic (IE) simulations for both flows. Some final remarks conclude the paper.

*Electronic address: D.Bernhardt@griffith.edu.au

†Electronic address: btodd@swin.edu.au

II. GENERAL FEATURES OF THE SYSTEMS UNDER STUDY

Using nonequilibrium molecular dynamics methods, we simulate two-dimensional systems of eight and 32 simple (i.e., pointlike) atoms undergoing PSF and PEF. The atoms interact via a pairwise additive WCA potential [7], which is a truncated and shifted version of the Lennard-Jones potential:

$$\phi(r_{ij}) = \begin{cases} 4\varepsilon\left[\left(\dfrac{\sigma}{r_{ij}}\right)^{12} - \left(\dfrac{\sigma}{r_{ij}}\right)^{6}\right] + \phi_c & \text{for } r_{ij} < r_c, \\ 0 & \text{for } r_{ij} > r_c, \end{cases} \quad (1)$$

where $r_{ij} = |\mathbf{q}_i - \mathbf{q}_j|$, where $\mathbf{q}_i$ is the position vector of particle i, ε is the well depth, and σ is the value at which the Lennard-Jones potential is zero. ϕ_c is the value of the unshifted potential at the cutoff distance $r_c = 2^{1/6}\sigma$, so that the WCA potential is continuous. We use reduced quantities, such that the reduced density is $\rho^* = \rho\sigma^3$, the reduced temperature is $T^* = k_B T/\varepsilon$, where k_B is the Boltzmann constant, the reduced energy is $E^* = E/\varepsilon$, and the reduced time is $t = t^*/[\sigma(m/\varepsilon)^{1/2}]$, where m is the mass of the particle. The reduced shear rate (see the following subsection) is $\dot{\gamma}^* = \dot{\gamma}\sigma(m/\varepsilon)^{1/2}$ and similarly for the reduced elongation rate $\dot{\varepsilon}^*$. For convenience we drop the asterisks and set $m = \sigma = \varepsilon = 1$.

A. SLLOD algorithm for planar shear flow

The SLLOD algorithm is a well-known procedure [8] used for the simulation of many-body systems under PSF. The equations of motion for a system of simple atoms with streaming velocity in the x direction and gradient in the y direction are

$$\dot{\mathbf{q}}_i = \frac{\mathbf{p}_i}{m} + \mathbf{i}\dot{\gamma}y_i,$$

$$\dot{\mathbf{p}}_i = \mathbf{F}_i - \mathbf{i}\dot{\gamma}p_{yi} - \alpha_\beta \mathbf{p}_i, \quad (2)$$

where m denotes the mass of the particle (we assume that all particles have the same mass), $\mathbf{q}_i$ is the laboratory position and $\mathbf{p}_i$ is the peculiar momentum (i.e., the momentum taken with respect to the streaming momentum $m\mathbf{u}$) of the particle i, $\mathbf{i}$ is the unit vector in the x direction, $\mathbf{F}_i$ is the total intermolecular force acting on particle i, $\dot{\gamma} = \frac{\partial u_x}{\partial y}$ is the shear rate, and α_β is the Gaussian multiplier. β denotes whether the kinetic temperature [isokinetic (IK)] or the total energy (IE) is held constant, so that

$$\alpha_{IK} = \frac{\displaystyle\sum_{i=1}^{N} \mathbf{F}_i \cdot \mathbf{p}_i - \dot{\gamma}p_{xi}p_{yi}}{\displaystyle\sum_{i=1}^{N} \mathbf{p}_i \cdot \mathbf{p}_i} \quad (3)$$

for IK simulations and

$$\alpha_{IE} = -\frac{\dot{\gamma}P_{xy}V}{\displaystyle\sum_{i=1}^{N} \frac{\mathbf{p}_i \cdot \mathbf{p}_i}{m}} \quad (4)$$

for IE, where V is the volume of the simulation box and P_{xy} is the xy component of the instantaneous pressure tensor, defined via the Irving-Kirkwood procedure [8]

$$\mathbf{P} = \frac{1}{V}\left(\sum_{i=1}^{N} \frac{\mathbf{p}_i\mathbf{p}_i}{m} + \sum_{i=1}^{N}\sum_{j>i}^{N} \mathbf{r}_{ij}\mathbf{F}_{ij}\right) \quad (5)$$

where $\mathbf{F}_{ij} = -\frac{\partial\phi_{ij}}{\partial\mathbf{r}_i}$ is the force on particle i due to particle j and $\mathbf{r}_{ij} = \mathbf{q}_i - \mathbf{q}_j$. To simulate a steady state consistently, the system must obey Lees-Edwards PBCs [8]. The adiabatic equations of motion are non-Hamiltonian, whereas the temporal periodicity in the boundary conditions makes the system nonautonomous [18].

B. SLLOD algorithm for planar elongation flow

To simulate a system undergoing planar elongational flow, we implement the SLLOD algorithm, as done in earlier work by Todd and Daivis [9,10] and Baranyai and Cummings [11], with expansion in the x direction and contraction in the y direction. The equations of motion for the system are

$$\dot{\mathbf{q}}_i = \frac{\mathbf{p}_i}{m} + \dot{\varepsilon}(\mathbf{i}x_i - \mathbf{j}y_i),$$

$$\dot{\mathbf{p}}_i = \mathbf{F}_i - \dot{\varepsilon}(\mathbf{i}p_{xi} - \mathbf{j}p_{yi}) - \alpha_\beta \mathbf{p}_i, \quad (6)$$

where $\mathbf{i}$ and $\mathbf{j}$ are the unit vectors in the x and y directions, respectively, and $\dot{\varepsilon} = \frac{\partial u_x}{\partial x} = -\frac{\partial u_y}{\partial y}$ is the elongation rate. In this case, α_β has the form

$$\alpha_{IK} = \frac{\displaystyle\sum_{i=1}^{N} \mathbf{F}_i \cdot \mathbf{p}_i - \dot{\varepsilon}(p_{xi}^2 - p_{yi}^2)}{\displaystyle\sum_{i=1}^{N} \mathbf{p}_i \cdot \mathbf{p}_i} \quad (7)$$

for IK simulations and

$$\alpha_{IE} = -\frac{\dot{\varepsilon}(P_{xx} - P_{yy})V}{\displaystyle\sum_{i=1}^{N} \frac{\mathbf{p}_i \cdot \mathbf{p}_i}{m}} \quad (8)$$

for IE, where P_{xx} and P_{yy} are the diagonal components of the instantaneous pressure tensor (5).

Kraynik and Reinelt [14] were the first to explain the conditions that have to be imposed over the periodicity of the simulation box to allow a reproducibility of the lattice cell. This reproducibility was exploited by Todd and Daivis [9,10] and Baranyai and Cummings [11] in the first steady-state NEMD simulations of indefinite PEF. These conditions were recently recast [12] in an elegant scheme, exploiting their analogy with the well-know Arnold cat map [13]. We use this latter formulation and impose "deforming-brick" PBCs [9] over the system. The adiabatic equations of motion are

Hamiltonian, but still nonautonomous because of the PBCs.

It has been shown [19] that it is necessary to reset the y component of the momentum of each particle at each time step to compensate for numerical roundoff errors, in a similar way that it is necessary to rescale or include a feedback mechanism to ensure that the kinetic energy or the total energy are kept constant when a Gaussian thermostat or ergostat is used. This procedure has no effect on the properties that are calculated. The roundoff error grows exponentially in the direction of contraction and is solely a consequence of finite precision numerics. If not constrained it will lead to a catastrophic unphysical phase transition in the fluid which is induced by the thermostat. In this work we rezero the total momentum at each time step, as proposed in [19].

We note there that there has recently been some debate over whether or not the SLLOD equations of motion are correct for elongational flow. Tuckerman *et al.* [20] and more recently Edwards and colleagues [21,22] suggest that the so-called GSLLOD equations of motion should be used. However, we disagree with this assertion. The GSLLOD algorithm is known to suffer from inconsistencies [23,24] and a formal mathematical proof that the SLLOD equations of motion are correct for elongational flow is forthcoming [25]; we refer readers to these references for greater detail.

III. DEFINITIONS AND METHODS

A. Definitions of Lyapunov exponents and the CPR

Consider the equation of motion of a dynamical system as

$$\dot{\mathbf{\Gamma}} = \mathbf{G}(\mathbf{\Gamma}, t) \tag{9}$$

where $\mathbf{\Gamma}(t) = [\mathbf{q}(t), \mathbf{p}(t)]^{\mathrm{T}}$ represents a vector in the phase space. We can define displacement vectors $\delta\mathbf{\Gamma}$ between two points in the phase space, i.e., $\delta\mathbf{\Gamma} = \mathbf{\Gamma}_1 - \mathbf{\Gamma}_2$. Taking the limit $\delta\mathbf{\Gamma} \rightarrow \mathbf{0}$, the vectors become tangent to the phase space trajectory and obey the linearized equation

$$\delta\dot{\mathbf{\Gamma}} = \mathbf{T} \cdot \delta\mathbf{\Gamma} \tag{10}$$

where $\mathbf{T}$ is the so-called stability matrix, given by $\partial\mathbf{G}/\partial\mathbf{\Gamma}$. A definition for the Lyapunov exponents λ_i that is practical for use in simulations is

$$\lambda_i = \lim_{t \rightarrow \infty} \lim_{\delta\mathbf{\Gamma} \rightarrow 0} \frac{1}{t} \frac{|\delta\mathbf{\Gamma}_i(t)|}{|\delta\mathbf{\Gamma}_i(0)|} \tag{11}$$

where $|\delta\mathbf{\Gamma}_i(t)|$ is the length of the displacement vectors at time t, and the displacement vectors are kept orthogonal. Lyapunov exponents are expressed in units of $1/t$.

The CPR [1,6,15] states that in the limit as $t \rightarrow \infty$, for every exponent λ_i there is a conjugate $\lambda_{i'}$ such that $\lambda_i + \lambda_{i'} = \chi$, where χ is constant for every i, i'. A small number of exponents, that does not grow with N, might be excluded due to their association with conserved quantities or if they correspond to displacement vectors in the direction of flow. Whereas it is possible to prove that CPR must hold [6,26] for a thermostatted system whose adiabatic equations of motion are Hamiltonian (as for systems under PEF), it is still under debate [15–17] whether some non-Hamiltonian systems such

as SLLOD PSF obey it. In Sec. IV we will show that divergences from CPR for PSF are higher than for PEF, for either IK or IE constrained dynamics, suggesting that CPR is violated for SLLOD PSF.

B. Simulation details and definitions for dynamical quantities of the systems

For our simulations, we choose convenient state points for a comparison between PSF and PEF results. Since for PEF the simulation box undergoes periodic contraction proportional to the exponential of the elongation rate, we choose a density $\rho = 0.3$ for both eight- and 32-particle systems. This prevents the system from violating the minimum image convention [8] when the unit lattice undergoes maximum contraction. The second scalar invariant Π [27], is defined as $2\dot{\gamma}^2$ for PSF and $8\dot{\varepsilon}^2$ for PEF. It is a measure of energy dissipation in a viscous fluid. Equal values of Π for PSF and PEF imply equivalent rates of energy dissipation and hence make direct comparisons between PSF and PEF simulations physically more meaningful. We simulate systems with $\Pi = 0.0$, 2.0, and 8.0, corresponding to $\dot{\gamma} = 0.0$, 1.0, and 2.0 for PSF and $\dot{\varepsilon} = 0.0$, 0.5, and 1.0 for PEF.

We use a fourth-order Gear predictor-corrector integrator to evaluate Eq. (11) and a Gram-Schmidt orthogonalization scheme [28,29] at each time step to preserve the orthogonality of the set of tangent vectors $\delta\mathbf{\Gamma}_i$. The length of the timestep we use is $\Delta t = 10^{-4}$ for eight and 32 particles, for a total simulation time of $t = 10\,000$ for eight particles and 2000 for 32, i.e., 10^8 total steps for eight particles and 2×10^7 for 32 particles. Each state point is sampled via ten independent runs starting from an initial fcc lattice, where for each run the initial momenta are chosen randomly. We note that the simulation times are much greater than those used previously in [1–6,15,16].

For IK simulations, we choose a temperature $T = 1.0$ and we run IE simulations at the average internal energy resulting from the corresponding IK simulation (i.e., the one at the same Π). The difference in the final temperature of IE simulations and the set temperature for IK were of order 7×10^{-3} for eight particles and 10^{-3} for 32 particles.

To be confident of the validity of our results, we use the definition of the phase space compression factor $\Lambda = \nabla_{\mathbf{\Gamma}} \cdot \dot{\mathbf{\Gamma}}$ and perform checks on the sum of all the exponents every $t = 100$. It is straightforward to show that the following relations hold for PSF:

$$\langle \Lambda_{\mathrm{IK}} \rangle = \sum_{i=1}^{2dN} \lambda_i = \left\langle -\alpha_{\mathrm{IK}}(dN-1) + \dot{\gamma} \frac{\sum_{i=1}^{N} p_{xi}p_{yi}}{\sum_{i=1}^{N} \mathbf{p}_i \cdot \mathbf{p}_i} \right\rangle \tag{12}$$

for IK simulations and

TABLE I. Summary of results for IK simulations at equilibrium and for PSF and PEF at different rates. λ_{max} and λ_{min} are the maximum and minimum Lyapunov exponents, $\Sigma\lambda_i$; $\lambda_i > 0$ is the sum of the positive Lyapunov exponents, max dev is the deviation [Eqs. (12) and (14)] expressed as a percent of the sum of the max and min Lyapunov exponents, η_{NEMD} is the viscosity calculated with NEMD simulations [Eqs. (16) and (17)], η_L is the viscosity calculated with Eqs. (18) and (19), η_{CPR} is the viscosity calculated using the CPR for the maximum and minimum Lyapunov exponents, and D_{KY} is the Kaplan-Yorke dimension from Eq. (20). Uncertainties at 2σ where σ is the standard error, are next to the value of each quantity.

N	Type	Rate	α		λ_{max}		λ_{min}		$\Sigma\lambda_i$; $\lambda_i > 0$		max dev(%)	η_{NEMD}		$\eta_{L(sum)}$		$\eta_{L(max)}$		D_{KY}	
8	Equil.				1.776	0.003	−1.774	0.003	14.91	0.03								27.0	0.1
	PSF	1.0	0.408	0.002	1.751	0.002	−2.148	0.002	13.45	0.03	0.25	0.199	0.001	0.199	0.008	0.238	0.002	24.3	0.1
		2.0	1.241	0.005	1.784	0.003	−3.008	0.004	12.01	0.04	0.15	0.151	0.001	0.161	0.003	0.184	0.001	20.6	0.1
	PEF	0.5	0.442	0.001	1.795	0.003	−2.229	0.003	15.61	0.03	0.24	0.216	0.001	0.238	0.003	0.260	0.004	24.2	0.1
		1.0	1.360	0.003	1.910	0.002	−3.250	0.003	16.66	0.04	0.14	0.166	0.001	0.188	0.001	0.201	0.001	20.8	0.1
32	Equil.				1.960	0.003	−1.958	0.003	63.99	0.17								123.0	0.3
	PSF	1.0	0.394	0.001	1.951	0.004	−2.340	0.004	56.47	0.17	0.18	0.225	0.001	0.225	0.004	0.233	0.005	111.2	0.3
		2.0	1.130	0.003	1.984	0.007	−3.111	0.008	49.42	0.22	0.11	0.162	0.001	0.163	0.001	0.169	0.002	95.3	0.4
	PEF	0.5	0.430	0.001	1.976	0.006	−2.401	0.005	64.72	0.19	0.17	0.246	0.001	0.251	0.004	0.255	0.007	110.5	0.3
		1.0	1.259	0.001	2.066	0.005	−3.316	0.006	67.17	0.18	0.09	0.180	0.001	0.185	0.001	0.188	0.002	95.8	0.3

$$\langle\Lambda_{IE}\rangle = \sum_{i=1}^{2dN} \lambda_i = \left\langle -\alpha_{IE}(dN-2) + 2\dot{\gamma}\frac{\sum_{i=1}^{N} p_{xi}p_{yi}}{\sum_{i=1}^{N} \mathbf{p}_i \cdot \mathbf{p}_i} \right\rangle \quad (13)$$

$$\langle\Lambda_{IE}\rangle = \sum_{i=1}^{2dN} \lambda_i = \left\langle -\alpha_{IE}(dN-2) + 2\dot{\varepsilon}\frac{\sum_{i=1}^{N} (p_{xi}^2 - p_{yi}^2)}{\sum_{i=1}^{N} \mathbf{p}_i \cdot \mathbf{p}_i} \right\rangle \quad (15)$$

for IE simulations, where d is the dimension of the system (i.e., 2), N is the number of particles, and the angular brackets denote time averages over the steady state. We will refer to the second term in the right-hand side of Eqs. (12) and (13) as the deviation. In the same fashion, we have for PEF

$$\langle\Lambda_{IK}\rangle = \sum_{i=1}^{2dN} \lambda_i = \left\langle -\alpha_{IK}(dN-1) + \dot{\varepsilon}\frac{\sum_{i=1}^{N} (p_{xi}^2 - p_{yi}^2)}{\sum_{i=1}^{N} \mathbf{p}_i \cdot \mathbf{p}_i} \right\rangle \quad (14)$$

for IK simulations and

for IE simulations. In Tables I and II we indicate the maximum value of the deviation at the end of the runs as a percentage of the sum of the exponents, for each state point: the disagreement for each of the four above equations was at most 0.25% of the value of the sum at each check. The maximum difference does not change considerably after $t = 100$.

There is an established link between the sum of the Lyapunov exponents and the viscosity of systems under PSF or PEF. Defining the shear viscosity as

TABLE II. Summary of results for IE simulation at equilibrium and for PSF and PEF at different rates as in Table I. Results at $\Pi = 8.0$ for eight particles are absent because of the instability of the simulations.

| N	Type	Rate	α		λ_{max}		λ_{min}		$\Sigma\lambda_i$; $\lambda_i > 0$		max dev (%)	η_{NEMD}		$\eta_{L(sum)}$		$\eta_{L(max)}$		D_{KY}	
8	Equil.	0.0			1.776	0.004	−1.775	0.004	14.60	0.03								27.0	0.1
	PSF	1.0	0.461	0.002	1.792	0.003	−2.197	0.005	13.38	0.04	0.13	0.197	0.001	0.222	0.003	0.243	0.000	24.1	0.1
	PEF	0.5	0.497	0.001	1.818	0.002	−2.277	0.002	15.92	0.04	0.12	0.213	0.001	0.281	0.002	0.278	0.003	23.9	0.1
32	Equil.	0.0			1.958	0.004	−1.955	0.004	64.56	0.15								123.0	0.3
	PSF	1.0	0.394	0.001	1.961	0.004	−2.346	0.005	56.23	0.18	0.14	0.226	0.001	0.229	0.004	0.231	0.005	111.0	0.3
		2.0	1.130	0.003	2.131	0.007	−3.192	0.008	49.74	0.18	0.09	0.161	0.001	0.167	0.001	0.159	0.002	95.3	0.4
	PEF	0.5	0.439	0.001	1.987	0.005	−2.415	0.005	65.18	0.19	0.14	0.246	0.001	0.255	0.003	0.257	0.006	110.3	0.3
		1.0	1.293	0.003	2.221	0.005	−3.415	0.005	67.33	0.18	0.09	0.179	0.001	0.188	0.001	0.179	0.001	95.7	0.3
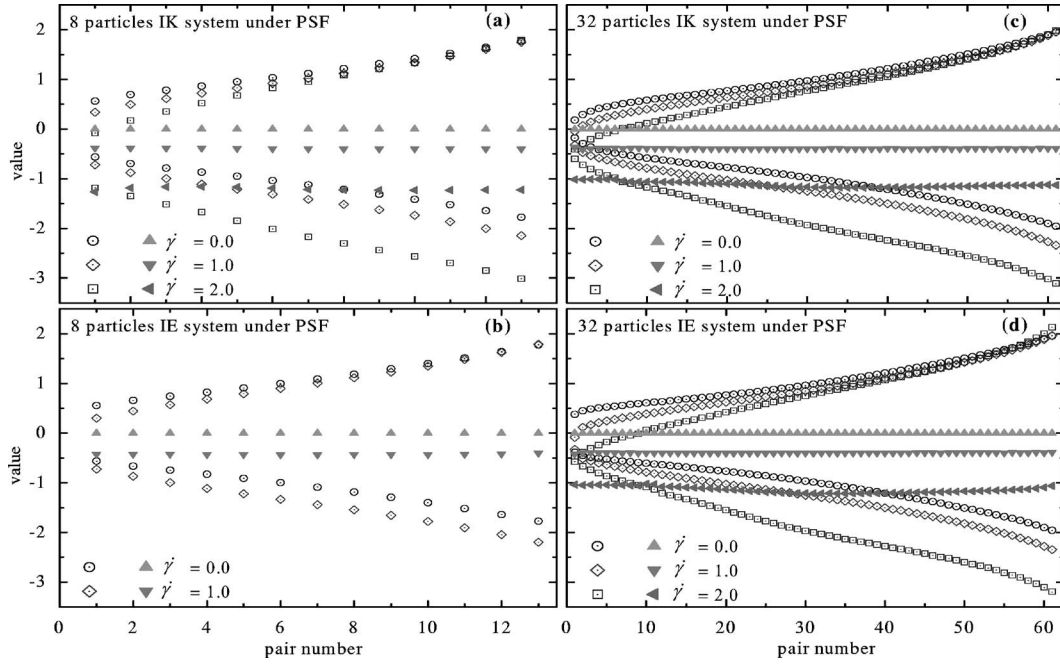
FIG. 1. Spectra of Lyapunov exponents for systems of eight and 32 particles in equilibrium and in a nonequilibrium steady state, at different shear rates. In (a), systems of eight particles undergoing isokinetic constrained dynamics are depicted. The values of exponents are indicated by open symbols; the values of the sums of pair numbers are indicated by filled triangles. In (b), eight particles under isoenergetic dynamics are represented. In (c), 32 particles under isokinetic dynamics and in (d), 32 particles under isoenergetic dynamics are shown.

$$\eta_{PSF} = -\frac{\langle P_{xy}\rangle}{\dot{\gamma}} \tag{16}$$

and the elongation viscosity as

$$\eta_{PEF} = -\frac{\langle P_{xx}\rangle - \langle P_{yy}\rangle}{4\dot{\varepsilon}} \tag{17}$$

it can be shown [30] that, neglecting terms of order $O(1/N)$, we have

$$\eta_{PSF} = -\frac{k_B\langle T\rangle}{\dot{\gamma}^2 V}\sum_{i=1}^{2dN}\lambda_i \tag{18}$$

for PSF systems and

$$\eta_{PEF} = -\frac{k_B\langle T\rangle}{4\dot{\varepsilon}^2 V}\sum_{i=1}^{2dN}\lambda_i \tag{19}$$

for PEF systems, where the angular brackets indicate a time average of temperature over the steady state. If we assume that the system obeys the CPR, we can replace the term for the sum of the exponents with a single sum of exponents of our choosing. For example, if we use the maximum and the minimum exponents we can substitute into Eq. (18) $\Sigma_{i=1}^{2dN}\lambda_i \rightarrow dN(\lambda_{max}+\lambda_{min})$. Results for viscosities from direct NEMD calculations [Eqs. (16) and (17)], from expressions involving the sum of the exponents [Eqs. (18) and (19)], and from application of CPR with $(\lambda_{max}+\lambda_{min})$ are shown in Tables I and II.
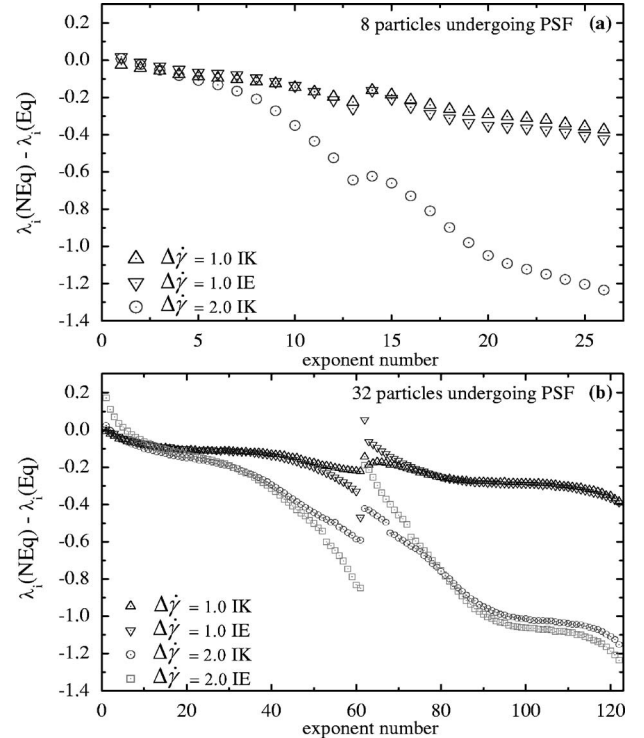

FIG. 2. Differences between the values of the exponents in a nonequilibrium steady state for PSF $[\lambda_i(\mathrm{NEq})]$ and the corresponding value at equilibrium $[\lambda_i(\mathrm{Eq})]$. In (a), systems of eight particles under isokinetic and isoenergetic dynamics are shown. In (b), systems of 32 particles are depicted: $\Delta\dot{\gamma}$ indicates the shift between equilibrium and nonequilibrium shear rates and IK (IE) shows the constrained dynamics.
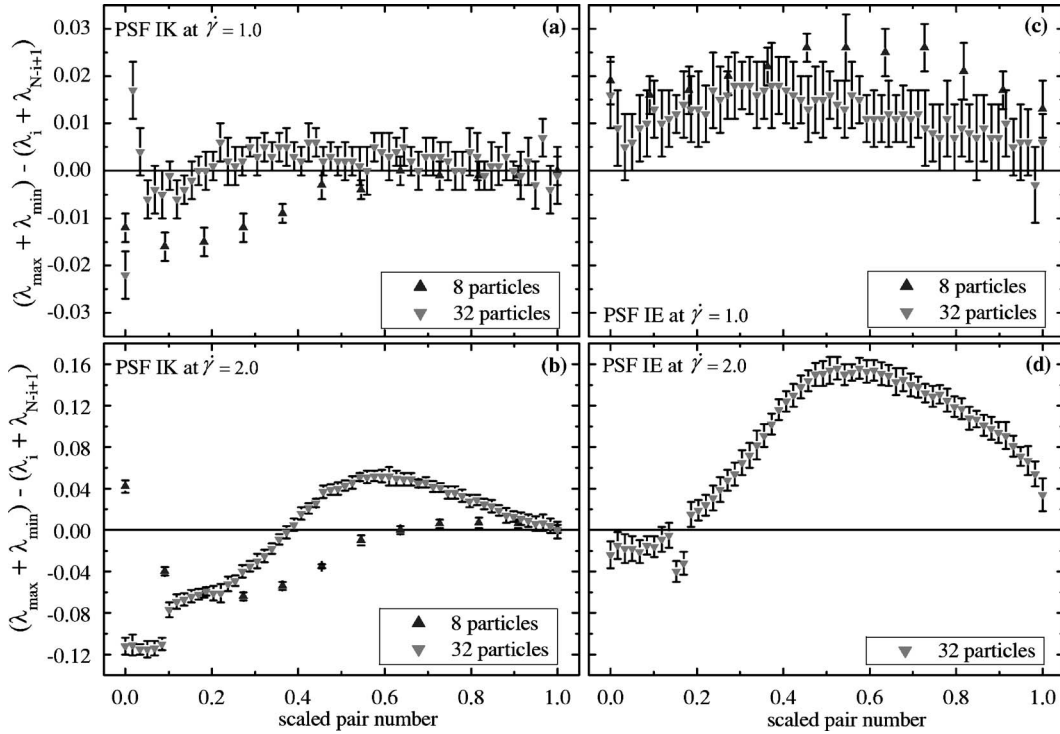
FIG. 3. Differences between the sum of maximum and minimum Lyapunov exponents and the sums of scaled pairs for systems of eight and 32 particles under planar shear flow at $\dot{\gamma}=1.0$ and 2.0. The values of the differences are indicated by filled triangles with error bars. Systems under isokinetic dynamics are in (a) and (b) and under isoenergetic dynamics in (c) and (d). Plots at the same shear rate have the same scale. The error bars are twice the standard error of the mean of ten independent runs.

Lyapunov exponents can be used to evaluate the fractal dimension of the attractor that the phase space collapses on when the system is in a steady state [2–5]. This dimension can be calculated using the Kaplan-Yorke conjecture [31], which leads to the following formula for the embedded dimension of the attractor in the phase space:

$$D_{KY} = M + \frac{\sum_{i=1}^{M} \lambda_i}{|\lambda_{M+1}|} \qquad (20)$$

where the exponents are ordered such that $\lambda_1 > \lambda_2 > \lambda_3 \cdots$ and M is the largest integer for which $\sum_{i=1}^{M} \lambda_i > 0$.

We finally point out that we are not able to perform simulations for IE dynamics at $\Pi = 8.0$ for eight-particle systems, for either flow. We observe that the system becomes unstable very soon in the simulation run with the time step used, as the ergostat fails to keep the total internal energy constant. We believe that this size-related effect is partly associated with the appearance of a string phase, which causes the particles in the system to travel in "stringlike" structures, minimizing the entropy [32]. This is an artifact that results from the action of the PBCs and the profile-biased Gaussian ergostat. These structures have relatively high potential energy and therefore adjustment of the momentum by the ergostat may not be sufficient to ensure that the energy remains constant. To our knowledge, this is the first time that this effect is noticed for the systems under study.

C. Lyapunov exponents associated with conserved properties of the systems

The actual phase space dimension of the systems under study is $(2dN - 2d - 1)$, where N is the number of particles, because fixed total momentum and either the kinetic or total internal energy of the systems are required, and a fixed center of mass is chosen. However, we note that if the total momentum or the center of mass is not initially zero, then they will not be necessarily conserved by Eqs. (2) and (6). If we wish to use arbitrary initial conditions, the equations of motion can easily be modified so that the total momentum and center of mass are conserved: $\mathbf{p}_i \rightarrow \mathbf{p}_i - (1/N)\Sigma_{i=1}^{N}\mathbf{p}_i$; $\mathbf{q}_i \rightarrow \mathbf{q}_i - (1/N)\Sigma_{i=1}^{N}\mathbf{q}_i$. While the dynamics of the trajectory will be unchanged by the transformation, the Lyapunov spectrum will, as the tangent trajectories in Eqs. (2) and (6) will not necessarily conserve the required quantities. The Lyapunov exponents associated with displacements in these directions will therefore be affected by this choice. Selection of the equations of motion to be examined is somewhat arbitrary, and here we choose to use the equations of motion in the form (2) and (6). An alternative approach is to prevent displacement vectors from pointing in directions orthogonal to the constraint planes. We prefer to consider the full $2dN$ phase space so that no false constraint is inadvertently imposed.

For simple tangent vectors, it is possible to determine (or approximate) the value of the Lyapunov exponents from direct consideration of the linearized tangent vector equations of motion Eq. (10). In terms of the "trivial exponents" asso-

ciated with the conserved quantities, it can be seen that there is an important distinction between PSF and PEF, due to the different symmetries of the respective equations of motions. Inspection of Eq. (2) for $\dot{\mathbf{q}}_i$ shows that no exponential separation of the trajectories results from translation of x and y components of the $\mathbf{q}_i$ and the Lyapunov spectrum presents two exponents that are exactly zero. On the other hand, the α term in $\dot{\mathbf{p}}_i$ in Eq. (2) results in two exponents whose values are $-\langle\alpha\rangle$

The dynamics of PEF given by Eq. (6) will be affected by translation of $\mathbf{q}_i$ and $\mathbf{p}_i$ and the trivial exponents have values $\dot{\varepsilon}$ and $-\dot{\varepsilon}$ for the $\dot{\mathbf{q}}_i$ term and $\dot{\varepsilon}-\langle\alpha\rangle$ and $-\dot{\varepsilon}-\langle\alpha\rangle$ for the $\dot{\mathbf{p}}_i$ term. The above values are independent of the type of constrained dynamics for either flows. Nevertheless in each case, these exponents produce two pairs that sum to $-\langle\alpha\rangle$.

The last two trivial exponents are associated with displacements orthogonal to the constant energy or temperature surface and parallel to the direction of flow. The exponent associated with displacement in the direction of flow is sometimes referred to as the "unpaired exponent" [1]. In autonomous systems it has value 0, while in nonautonomous systems, its value always seems to be related to $-\langle\alpha\rangle$, in either IK and IE constrained dynamics for either flow. Interestingly, the other exponent for this pair has different values for PSF and PEF, depending on the type of constrained dynamics.

Consider an initial displacement of $\delta\boldsymbol{\Gamma}$ in the direction orthogonal to the total energy or kinetic energy constraint surface of the system. If we imagine that $\mathbf{F}_i$ and α are neglected in the equations of motion, the value of the exponent can be roughly predicted if we look for the greatest exponential growth along the directions that change the constrained energy. In the case of PEF under IK, the constraint on the kinetic energy involves only the momenta and the dominant contribution will be from the y component of the $\dot{\mathbf{p}}_i$. This term is equal to $\dot{\varepsilon}-\alpha$, which is almost zero: the contribution is very small and the exponent is practically zero. In the case of PEF under IE dynamics [see Eq. (6)], a nonzero contribution comes from the x component of the $\dot{\mathbf{q}}_i$, because of the term $\dot{\varepsilon}x$. This causes the exponent to have a value similar to $\dot{\varepsilon}$, but not exactly equal because of the actual corrections due to the force and the (time-dependent) ergostat terms.

For PSF, no positive contributions are present in either IK and IE dynamics: the form of the right-hand side of Eq. (2) does not contain positive terms for $\dot{\mathbf{q}}_i$ or $\dot{\mathbf{p}}_i$ that can lead to an exponential growth so the value of the exponent in both cases is exactly zero.

It should be noticed that there might be some ambiguity in the way the last two trivial exponents are identified from the numerical data. This is particularly true in a system of 32 particles because the values of the exponents are very close to each other. In any case, variations are small and do not affect any of our conclusions.

IV. RESULTS AND DISCUSSION

We evaluate the spectra for PSF for $\Pi=0.0$, 2.0, and 8.0 in IK and IE constrained dynamics and present the cumulative spectra in Fig. 1, omitting the trivial exponents. A visual
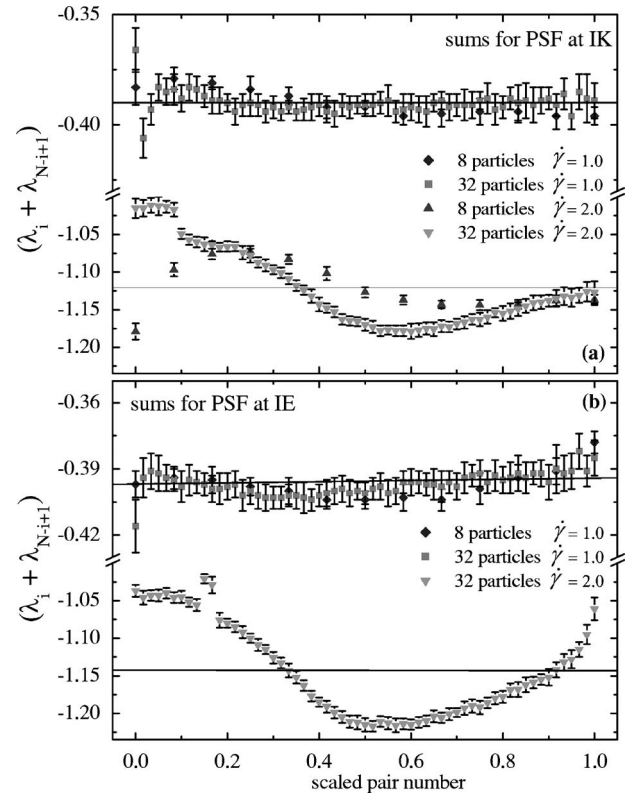

FIG. 4. Sums of exponents for eight and 32 particles in nonequilibrium steady-state conditions under PSF at different shear rates and constrained dynamics. The sums for the smaller system are shifted appropriately to take size effects into account. (a) shows systems under isokinetic and (b) under isoenergetic dynamics. The error bars represent twice the standard error of the mean of ten independent runs.

inspection of Fig. 1 shows good agreement with previous findings [16]: the deviation from CPR increases as we go from $\dot{\gamma}=1.0$ to $\dot{\gamma}=2.0$. For eight-particle IK and IE simulations [Figs. 1(a) and 1(b)] and for 32-particle IK and IE simulations [Figs. 1(c) and 1(d)] the sum of the exponents (filled triangles) at $\dot{\gamma}=2.0$ shows deviations from linearity in low pair numbers (beginning of the spectra) and tends to increase for high pair numbers.

In Fig. 2 we plot the differences between the value of the exponents in nonequilibrium states and the corresponding value at equilibrium, neglecting the unpaired exponent. The maximum exponent has the label 1, the second highest has the label 2, and so on. For eight particles [Fig. 2(a)], our IK results agree with those of Fig. 2 in [1], showing a practically linear shift proportional to the exponent number. IE data for eight particles show a behavior quite similar to IK results, although the shift is more marked at the end and less prominent at the beginning. For 32 IK particles [Fig. 2(b)], differences are almost linear for $\dot{\gamma}=1.0$, but linearity is lost at $\dot{\gamma}=2.0$, with the appearance of a jump for medium exponent numbers and a steeper curvature than for $\dot{\gamma}=1.0$. For 32 IE particles [Fig. 2(b)], the jump is present also for $\dot{\gamma}=1.0$ and seems to increase linearly with the shear rate. In general, the width of the jump and the steepness of the curvature are greater for nonequilibrium states in IE than for states in IK.
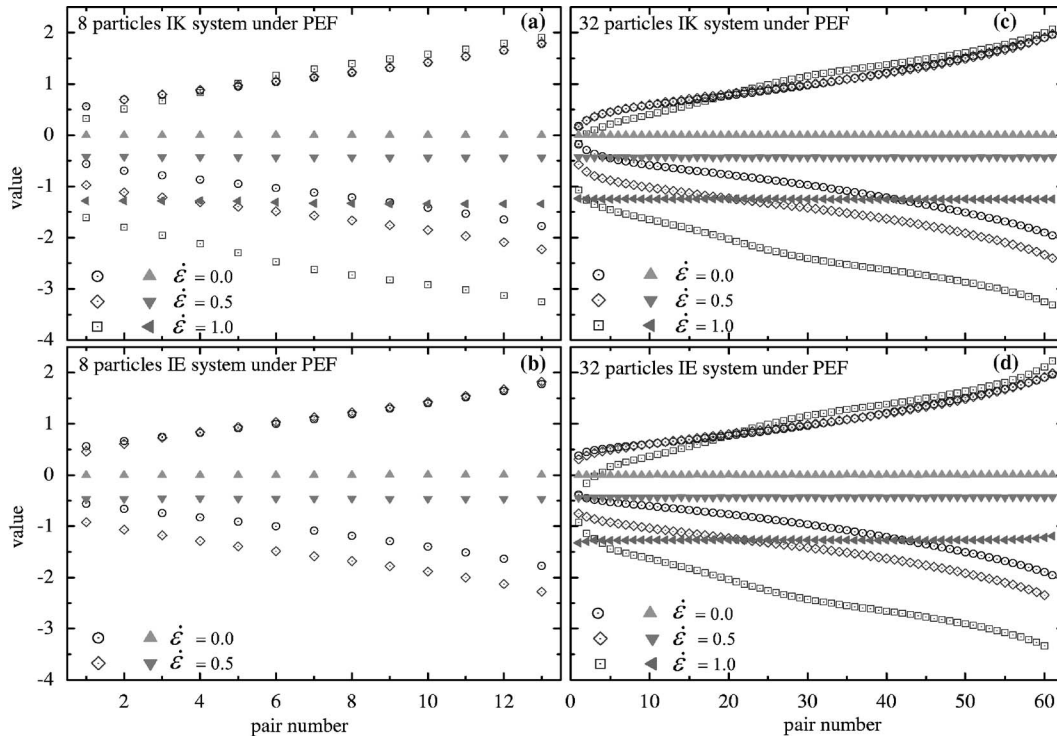
FIG. 5. Spectra of Lyapunov exponents for systems of eight and 32 particles in equilibrium and in a nonequilibrium steady state, at different elongational rates. In (a), systems of eight particles undergoing isokinetic constrained dynamics are depicted. The values of exponents are indicated by open symbols; the values of the sums of pair numbers are indicated by filled triangles. In (b), eight particles under isoenergetic dynamics are represented. In (c), 32 particles under isokinetic dynamics and in (d) 32 particles under isoenergetic dynamics are shown.

Furthermore, differences in IE data in lower exponent numbers are positive, whereas for IK they are almost zero for $\dot{\gamma}=1.0$ and negative for $\dot{\gamma}=2.0$.

To thoroughly test the CPR, we plot the differences between the sum of the maximum and minimum exponents $(\lambda_{max}+\lambda_{min})$ and the other pairs in Fig. 3 and rescale the pair numbers to compare systems of different sizes. Pair number 1.0 corresponds to the second highest and the second lowest exponent, following then the same order as Fig. 1.

In the first plot [Fig. 3(a)], a small deviation from CPR is evident in some pairs of exponents. On average, the deviation is less than 2% of $(\lambda_{max}+\lambda_{min})$ for eight particles and less than 1% for 32, tending to zero with the increase of pair number. Whereas there is a size-related effect for low pair numbers, there is no clear evidence for the same effect in the very first pair numbers, as they remain high for eight and 32 particles alike. For $\dot{\gamma}=2.0$ [Fig. 3(b)], the maximum deviation is around 5% for eight and 10% for 32 particles, with an average about 2.5% for eight and 4% for 32 particles.

A similar trend is seen for IE simulations [Figs. 3(c) and 3(d)], with higher average deviations than IK: about 5% for $\dot{\gamma}=1.0$ for eight particles and 3% and 8.5% for $\dot{\gamma}=1.0$ and 2.0 for 32 particles. The differences mainly reside in the positive domain, as for IE dynamics $(\lambda_{max}+\lambda_{min})$ is the largest of all the sums. We stress that the maximum deviation for IE simulations is around 5% and 15% for 32 particles at $\dot{\gamma}=1.0$ and 2.0 respectively, and about 6.5% for eight particles at $\dot{\gamma}=1.0$.

Finally, we plot the sum of exponents for PSF in Fig. 4. To take size dependence into account, the data for the smaller system is modified so that we have a meaningful comparison with the data for the larger system. In fact, we shift the data for the former so that the mean value of the sum of pairs for the smaller system is equal to that of the larger system. The scaled pair number index runs from 0 to 1 independently of N, where the index corresponding to the maximal and minimal exponent pair is 1, as in [15]. Generally, violations of the CPR increase with strain rate for both IK and IE PSF dynamics and are higher in IE dynamics. Maximum divergences are up to 10% of the average value of the sums at high shear rate and cannot be attributed to small-size effects, as one can clearly see from the plots.

Results for PEF are different. We plot the cumulative spectra in Fig. 5. Note that the y-axis scale is somewhat reduced compared to the corresponding PSF data in many cases. The sums show some divergence, but it decreases greatly with increasing N as expected, except the ones for 32 particles undergoing IE dynamics [Fig. 5(d)], where the sum for $\dot{\varepsilon}=1.0$ shows a symmetric shift at both edges. Nonetheless, we notice that the majority of the pair numbers show a linear behavior and follow CPR very well. There are two interesting features in Fig. 5. First, in the positive part of the spectra the nonequilibrium branch crosses the equilibrium one at around one-third of the spectrum and then stays above it as the exponent number increases. Second, the negative nonequilibrium exponents undergo a roughly constant shift with respect to the equilibrium values, which is approximately proportional to the square of $\dot{\varepsilon}$ in either constrained dynamics. If CPR is obeyed, and the positive exponents do

not change greatly, this shift will be equal to the value of the thermostat multiplier, to $O(1/N)$. Futhermore, examination of Eqs. (8) and (17) shows that in the linear regime α will vary as $\dot{\varepsilon}^2 \eta$.

These trends are also reflected in Fig. 6, where we plot differences in the same fashion as in Fig. 2. In Fig. 6(a), eight particles show an almost constant shift at $\Pi = 2.0$ for high exponent numbers and a symmetric curve for $\Pi = 8.0$. Figures 6(a) and 6(b) are interesting in that they seem to show a mirror inversion symmetry at the discontinuity at exponent number 13 for the former and at exponent number 60 for the latter. This is expected if CPR is obeyed. At equilibrium, the upper and lower arms of the spectrum will be related by a factor -1, whereas away from equilibrium they will be related by multiplication by -1 and subtraction of a constant. Therefore the difference between the equilibrium and nonequilibrium results will produce arms that are related by a reflection and a shift. Some semblance of this symmetry is also observed in Fig. 2.

In Fig. 6(b), 32 particles denote a less prominent slope for medium exponent numbers if compared with Fig. 2(b). The jump is in general higher for PEF, except for $\Pi = 2.0$ IE simulations. These observations are in agreement with Figs. 3 and 4 of [1], which show analogous features for DOLLS PSF, which has adiabatic Hamiltonian equations like those of SLLOD PEF.

Differences between $(\lambda_{\max} + \lambda_{\min})$ and the other pairs are plotted in Fig. 7. Consideration of the data for the IK dynamics [Figs. 7(a) and 7(b)] suggests that for large systems the CPR will be obeyed. At a system size of $N = 32$, very small departure from CPR is still observed, which is consistent with the results obtained for the DOLLS equations of motion [1,15]. These departures can be attributed to the expected $O(1/N)$ deviations of Gaussian thermostatted nonautonomous equations of motion, but the results indicate that CPR will be satisfied in the large-system limit, as predicted by noting the symplectic nature of the unthermostatted equations of motion. At low fields, the IE results are similar to those for IK dynamics. The deviation from pairing for IK dynamics [Figs. 7(a) and 7(b)] is on average 1.4% and 2.1% for eight particles for $\dot{\varepsilon} = 0.5$ and 1.0 respectively, dropping remarkably to 0.4% and 0.3% on average for 32 particles at the same elongational rates. Moreover, maximum deviations are around 1% for 32 particles under PEF IK. This can be compared with maximum deviations of approximately 10% for a PSF system with similar dissipation. Also, the greatest occurrence of divergence is concentrated in the first part of the spectrum [Fig. 7(b)], with an evident $1/N$ dependence for either rates [Figs. 7(a) and 7(b)]. This trend is absent in PSF, as high divergences (as previously noted) take place in the middle of the spectrum (see Fig. 3(b)).

IE simulations show a good agreement with CPR for $\dot{\varepsilon} = 0.5$ [Fig. 7(c)] with an average deviation around 0.8% for eight particles and 0.9% for 32 particles. A maximum divergence of 1.9% is present in eight particles and the first difference for 32 particles has a divergence of 3.3%, but there is a clear size-related behavior for increasing pair-numbers. For $\dot{\varepsilon} = 1.0$ [Fig. 7(d)], divergence is higher, but almost constant on the average. This is due to the fact that $(\lambda_{\max} + \lambda_{\min})$ is the highest sum of all. In any case, the highest deviation from
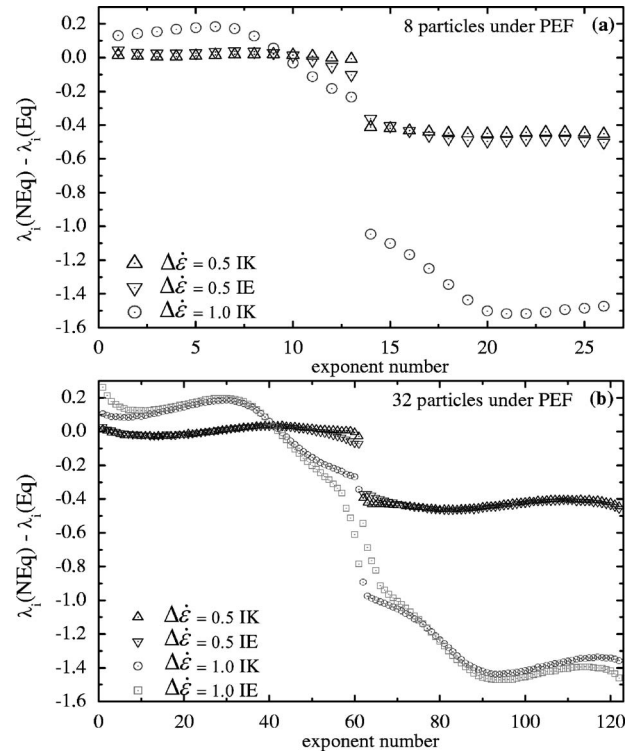

FIG. 6. Differences between the values of the exponents in a nonequilibrium steady-state for PEF $[\lambda_i(\text{NEq})]$ and the corresponding value at equilibrium $[\lambda_i(\text{Eq})]$. In (a), systems of 8 particles under isokinetic and isoenergetic dynamics are shown. In (b), systems of 32 particles are depicted: $\Delta\dot{\varepsilon}$ indicates the shift between equilibrium and nonequilibrium elongational rates and IK/IE shows the constrained dynamics.

the mean sum is just around 5% and concentrated in few exponents at very low or very high pair numbers.

All these features are also evident in Fig. 8 where, apart from small size-dependant deviations, CPR is obeyed for $\Pi = 2.0, 8.0$ for IK simulations and for IE simulations violations are only observed at the beginning and at the end of the spectra. These violations appear only at high elongation rate.

On the other hand, we note that deviations for PSF are present independent of the shear rate or the dynamics: maximum deviations from the mean of sums increase for IK dynamics from 2% and 5% for eight particles to 9% and 10% for 32 particles at $\Pi = 2.0, 8.0$ respectively. For IE dynamics at $\Pi = 2.0$ they are 5% for eight particles and 32 particles alike and 10% for 32 particles at $\Pi = 8.0$. These deviations do not seem to be removed either by increasing the size or by changing the thermostatting mechanism.

We conclude this section with three final observations. In Tables I and II, we collate data for the systems under study. As we expect, Eqs. (18) and (19) give values for viscosities for PSF and PEF which are in good agreement with results from direct NEMD calculations only if the system is sufficiently large, clearly showing $1/N$ dependence. Even when CPR is not satisfied, using $(\lambda_{\max} + \lambda_{\min})$ to simplify the formula for viscosities gives good results, as noticed in [15].

Next, we note that there are no significant differences out of statistical uncertainties between the Kaplan-Yorke dimen-
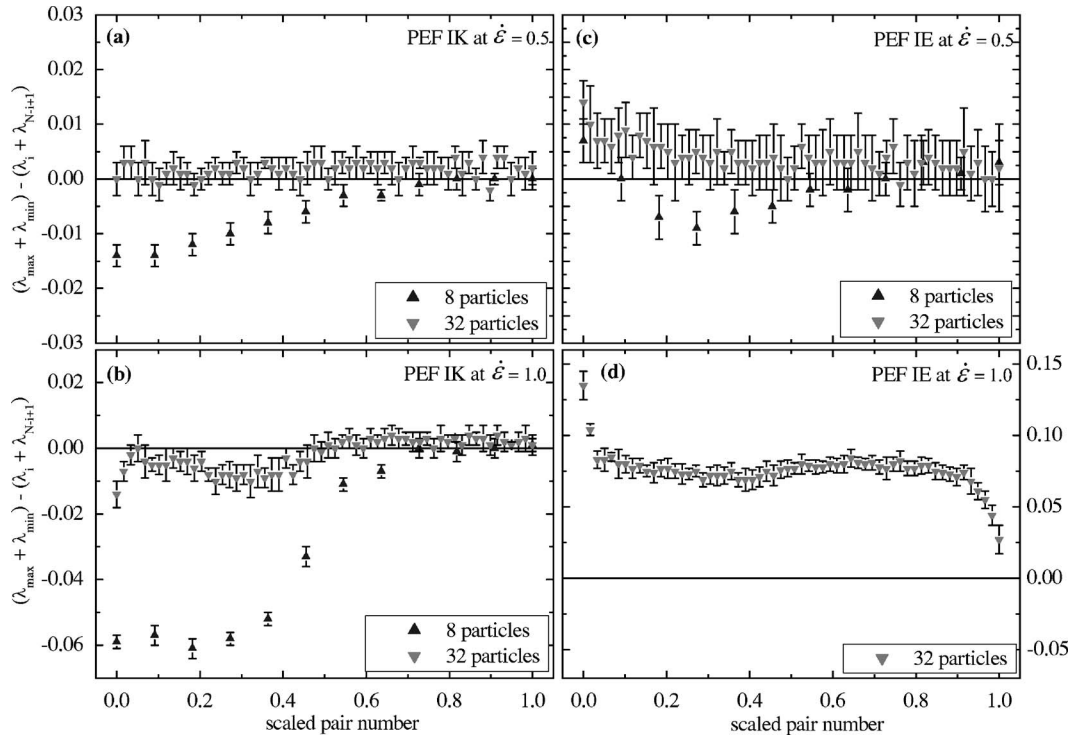
FIG. 7. Differences between the sum of maximum and minimum Lyapunov exponents and the sums of scaled pairs for systems of eight and 32 particles under PEF at $\dot{\varepsilon}=0.5$ and 1.0. The values of the differences are indicated by filled triangles with error bars. Systems under isokinetic dynamics are in (a) and (b) and under isoenergetic dynamics in (c) and (d). Plots at $\dot{\varepsilon}=0.5$ have the same scale; plots at $\dot{\varepsilon}=1.0$ have different scales. The error bars represent twice the standard error of the mean of ten independent runs.

sions of analogous PEF and PSF phase space points in the same regimes. Thus we conclude that the phase space undergoes a similar contraction for both flows, only dependent on the second scalar invariant Π in the linear regime.

Finally, we make an interesting observation about the chaoticity of PSF and PEF systems. It has recently been suggested [24] that PEF is an inherently more chaotic flow than PSF, based upon the relationship of the Arnold cat map and the convective part (i.e., the macroscopic streaming momentum) of PEF that the cat map effectively describes. The cat map has a relatively large positive Lyapunov exponent, indicating a chaotic macroscopic flow, whereas the corresponding dynamical map for the convective part of the flow for PSF [12] has zero Lyapunov exponent, indicating no macroscopic chaos, even though from a microscopic perspective both flows are of course chaotic. It was thus suggested that the superposition of a chaotic convective flow and chaotic microscopic dynamics for PEF would make PEF an inherently more unstable flow than PSF. In Fig. 9 we plot the sum of the positive exponents for the IE and IK systems studied and find that indeed it is always greater for PEF than PSF. Indeed, as strain rate increases, this measure of the chaoticity for PSF decreases as expected, but *increases* for PEF for increasing elongational rate, which may reflect the fact that for elongational flow an external field must exist to maintain the flow. It is this field that leads to hyperbolic streaming velocity profiles and exponentially diverging or converging points in space, which contribute to a greater degree of microscopic chaos at higher rates of elongation. For PSF, no such external field is present at $t>0$ and a resulting decrease

in this measure of chaoticity is observed, which may be because there is no direct contribution to the Lyapunov exponents from the macroscopic streaming velocity. Also the maximum Lyapunov exponent is always greater for PEF, as can be seen from Tables I and II. While not a rigorous proof of this conjecture, these considerations do lend support to it. This in turn adds further weight to the observations made earlier by Todd and Daivis [19] that sensitive dependence to initial conditions is critical for numerical stability in NEMD simulations of PEF, whereas they are nowhere as important for equivalent PSF simulations.

V. CONCLUSIONS

In this paper we have presented an extensive analysis of the chaotic properties of many-body systems of simple atoms in a nonequilibrium steady state, driven either by a planar shear or elongational flow and undergoing either isokinetic or isoenergetic constrained dynamics. The comparison between numerical data shows that the conjugate-pairing rule (small size-related effects aside) clearly holds for SLLOD equations of motion for elongational flow, whereas the convergence for SLLOD equations for shear flow is definitely problematic. This is the first time, to our knowledge, that numerical data support the fact that the conjugate-pairing rule is obeyed by planar elongational flow, given the Hamiltonian nature of the governing adiabatic equations of motion.

Furthermore, given the same rate of energy dissipation, the nonequilibrium phase space contraction is the same for either type of flow, but systems under planar elongational
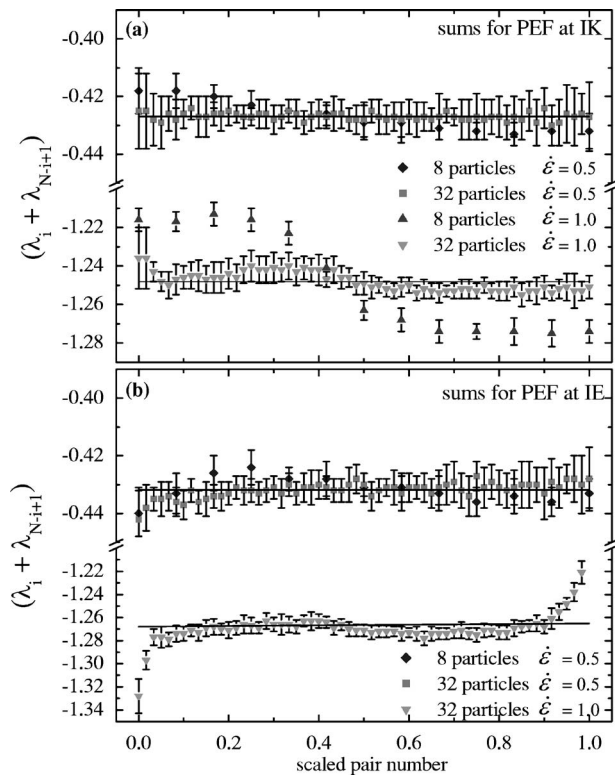
FIG. 8. Sums of exponents for eight and 32 particles in a nonequilibrium steady state under PEF at different elongation rates and constrained dynamics. The sums for the smaller system are shifted appropriately to take size effects into account: (a) shows systems under isokinetic and (b) under isoenergetic dynamics. The error bars represent twice the standard error of the mean of ten independent runs.

flow show greater maximum exponents and bigger sums of the positive Lyapunov exponents and hence exhibit an intrinsically more chaotic nature. Although the periodic boundary conditions for planar elongational flow imposed over the unit lattice are intimately related to the well-known Arnold cat map, which is in turn related to the chaotic nature of the convective part of the flow, there is no clear evidence of the presence of the map in the Lyapunov spectra we proposed.
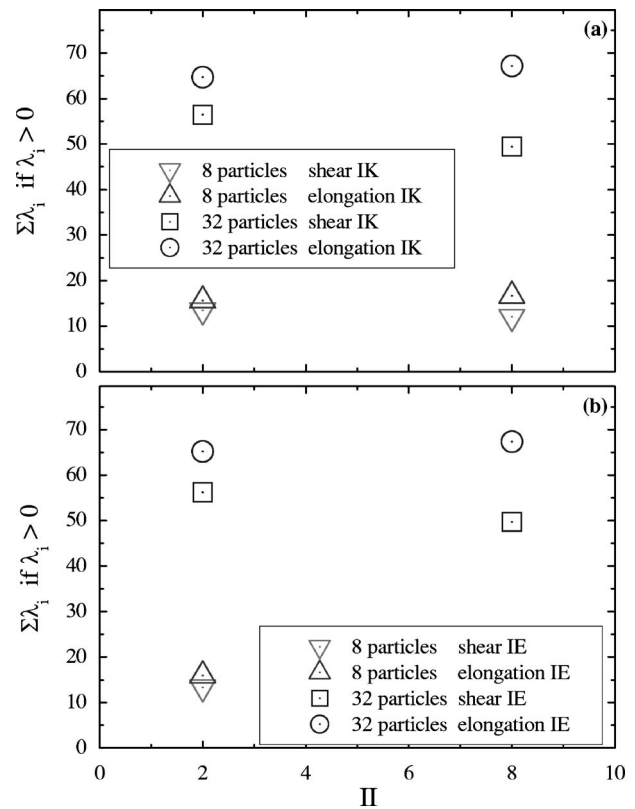

FIG. 9. Sums of the positive Lyapunov exponents for the systems under consideration: (a) shows isokinetic and (b) isoenergetic constrained dynamics.

The actual existence of such an "imprint" and its eventual relation with the so-called unpaired exponent in the Lyapunov spectra are objects of a forthcoming study.

ACKNOWLEDGMENTS

[1] S. Sarman, D. J. Evans, and G. P. Morriss, Phys. Rev. A **45**, 2233 (1992).

[2] G. P. Morriss, Phys. Lett. A **134**, 307 (1989).

[3] G. P. Morriss, Phys. Rev. A **37**, 2118 (1988).

[4] H. A. Posch and W. G. Hoover, Phys. Rev. A **38**, 473 (1988).

[5] H. A. Posch and W. G. Hoover, Phys. Rev. A **39**, 2175 (1989).

[6] D. J. Evans, E. G. D. Cohen, and G. P. Morriss, Phys. Rev. A **42**, 5990 (1990).

[7] J. D. Weeks, D. Chandler, and H. C. Anderson, J. Chem. Phys. **54**, 5237 (1985).

[8] D. J. Evans and G. P. Morriss, *Statistical Mechanics of Nonequilibrium Liquids* (Academic, New York, 1990).

[9] B. D. Todd and P. J. Daivis, Comput. Phys. Commun. **117**, 191

[10] B. D. Todd and P. J. Daivis, Phys. Rev. Lett. **81**, 1118 (1998).

[11] A. Baranyai and P. T. Cummings, J. Chem. Phys. **110**, 42 (1999).

[12] T. A. Hunt and B. D. Todd, Mol. Phys. **101**, 3445 (2003).

[13] V. I. Arnold, *Mathematical Methods of Classical Mechanics* (Springer-Verlag, New York 1989).

[14] A. M. Kraynik and D. A. Reinelt, Int. J. Multiphase Flow **18**, 1045 (1992).

[15] D. J. Searles, D. J. Evans, and D. J. Isbister, Chaos **8**, 337 (1998).

[16] G. P. Morriss, Phys. Rev. E **65**, 017201 (2001).

[17] D. Panja and R. van Zon, Phys. Rev. E **66**, 021101 (2002).

(1999).

[18] J. Petravic and D. J. Evans, Mol. Phys. **95**, 219 (1998).

[19] B. D. Todd and P. J. Daivis, J. Chem. Phys. **112**, 40 (2000).

[20] M. E. Tuckerman, C. J. Mundy, S. Balasubramanian, and M. L. Klein, J. Chem. Phys. **106**, 5615 (1997).

[21] B. J. Edwards and M. Dressler, J. Non-Newtonian Fluid Mech. **96**, 163 (2001).

[22] C. Baig, B. J. Edwards, D. J. Keffer, and H. D. Cochran, J. Chem. Phys. **122**, 114103 (2005).

[23] D. J. Evans, D. J. Searles, W. G. Hoover, C. G. Hoover, B. L. Holian, H. A. Posch, and G. P. Morriss, J. Chem. Phys. **108**, 4351 (1998).

[24] B. D. Todd, Mol. Simul. **31**, 411 (2005).

[25] P. J. Daivis and B. D. Todd, J. Chem. Phys. (to be published).

[26] C. P. Dettmann and G. P. Morriss, Phys. Rev. E **53**, R5545 (1996).

[27] R. B. Bird, R. C. Armstrong, and O. Hassager, *Dynamics of Polymeric Liquids* (Wiley, New York, 1987), Vol. 1.

[28] I. Shimada and T. Nagashima, Prog. Theor. Phys. **61**, 1605 (1979).

[29] G. Benettin, L. Galgani, A. Giorgilli, and J. M. Strelcyn, Meccanica **15**, 9 (1980).

[30] E. G. D. Cohen, Physica A **213**, 293 (1994).

[31] P. Frederickson, J. L. Kaplan, and E. D. Yorke, J. Diff. Eqns. **49**, 185 (1983).

[32] D. J. Evans and G. P. Morriss, Phys. Rev. Lett. **56**, 2172 (1986).